https://doi.org/10.5194/egusphere-2025-5066
Preprint. Discussion started: 27 March 2026

Study on Dynamic Data Transmission Technology for Expendable Current Profiler

Keyu Zhou[1], Fei Zhang[1,*], Lihua Liu[1], Zhaohui Peng[1], Donghui Li[1], Dong Liu[1], Xingyuan Jiang[2] and Qisheng Zhang[2]

[1]Institute of Acoustics, Chinese Academy of Sciences, Beijing, China
[2]School of Geophysics and Information Technology, China University of Geosciences (Beijing), Beijing, China

Correspondence to: Fei Zhang (e-mail: zhangfei@mail.ioa.ac.cn)

Abstract. Expendable Current Profilers (XCPs) play a crucial role in global ocean parameter detection and deep-sea physical oceanography research. However, affected by the complex seawater environment and the dynamic impedance changes of enamelled wires during probe deployment, such expendable devices face bottlenecks in long-distance dynamic data transmission. Specifically, they suffer from high transmission bit error rates (approximately 10^{-2}), limited transmission distances (around 1 km), and low transmission rates (2400 baud or 4800 baud). These issues severely restrict their development and practical application. To address the aforementioned bottlenecks, this study conducted targeted research focusing on the optimization of data transmission technology. It effectively reduced transmission interference by optimizing the analog circuit design for Low-Voltage Differential Signaling (LVDS) data transmission. Additionally, RS encoding technology was added to the digital board of the probe to lower the transmission bit error rate. Experimental verification shows that the optimized system can achieve data transmission over a distance of 2500 meters using a double-coated enamelled wire with a diameter of 0.1 mm. The data transmission rate is increased to 9600 baud, and the bit error rate is reduced to 10^{-4}, resulting in a significant improvement in overall performance. Furthermore, the system operates stably and reliably, with all functions meeting the preset design requirements, laying a foundation for subsequent practical marine applications.

1 Introduction

Expendable Marine Environmental Parameter Profilers (XMEP) such as Expendable Current Profiler (XCP), Expendable Conductivity, Temperature, and Depth (XCTD) profiler, and Expendable Bathythermograph (XBT), play a crucial role in global ocean parameter profiling, providing significant support for deep-sea physical oceanography research. These devices can be deployed at desired measurement points from moving ships or aircraft without the need for recovery or halting operations, offering convenient and efficient operation (Hannon et al., 2000). The earliest type of expendable marine profiler, the XBT, was developed to measure seawater temperature and depth (Justine et al., 2002). With the growing demand for enhanced functionality and continuous improvements by researchers, various other expendable marine

https://doi.org/10.5194/egusphere-2025-5066
Preprint. Discussion started: 27 March 2026

instruments have been developed, including the XCTD (Sijia et al., 2024; Li et al., 2019), the Expendable Sound Velocity (XSV) profiler (Fan et al., 2019), and the XCP (Sanford et al., 1971; Sanford et al., 1978). These instruments are widely used in both military and commercial sectors due to their ease of use and rapid deployment, which is critical for the collection of temperature, salinity, depth, sound velocity, and current speed data. Such data are vital for ocean safety, communication, navigation, and economic activities (Hongfeng et al., 2022; Long et al., 2021; Alvarinho et al., 2021). However, a common challenge faced by expendable marine environmental parameter profilers is long-distance dynamic data transmission, particularly the transmission from the probe to the buoy (or deck receiving unit). This dynamic data transmission often becomes a critical limiting factor in their development.

Research on dynamic data transmission for XMEP is relatively limited. Zhang et al. (Zhang et al., 2011) were the pioneers in proposing a dynamic data transmission technique for XCP. Their study designed a baseband transmission system utilizing digital baseband signal transmission technology. The test results indicated that this transmission system could achieve a distance of 1800 meters on a 0.1mm diameter enamelled wire, with the probe descending at a speed of 4 m/s and a transmission rate of 2400 bps. In 2017, Li et al. (Li et al., 2017) enhanced this technique by adopting Low-Voltage Differential Signaling (LVDS) as the physical layer for data transmission. They modified and optimized the data transmission protocol based on the RS232 standard and incorporated Manchester coding. Their laboratory and marine test results demonstrated that the designed system could achieve a data transmission distance of up to 2 km using a 0.1 mm diameter enamelled wire with 4800 bps baud rate. In 2023, Zhou et al. (Zhou et al., 2023) developed an XCP that employed a data transmission technology with a baud rate of 4800bps and a transmission distance of 1.5km. The probe's data transmission process utilized a Universal Asynchronous Receiver/Transmitter (UART) protocol with one start bit, eight data bits, and one stop bit. The transmitter's physical layer used a Low-Voltage Differential Signaling transmitter on a System-on-a-Programmable-Chip (SoPC). However, due to the complex nature of seawater and the dynamic impedance changes in the enamelled wire caused by the expendable probe's deployment, the system faced challenges such as high transmission error rates (around 10^{-2}), limited transmission distances (within 2 km), and relatively slow transmission speeds (2400 bps or 4800 bps).

To address the aforementioned challenges, this study takes XCP as an example to introduce advanced encoding and decoding techniques, aiming to enhance the data transmission technology for XMEPs. Specifically, we optimized the hardware circuit and employed Low-Voltage Differential Signaling (LVDS) for data transmission. By providing a direct current path for the bias current in the AC coupling circuit at the signal reception front-end, we were able to increase the baud rate of dynamic data transmission, thereby improving both the signal transmission rate and quality. The use of RS encoding and decoding technology for data transmission significantly reduced the transmission error rate to 10^{-4}, extended the transmission distance to 2.5 km, and increased the transmission speed to 9600 bps. These advancements establish a robust foundation for the expendable marine environmental parameter profiler technology, enabling higher resolution and deeper ocean exploration.

https://doi.org/10.5194/egusphere-2025-5066
Preprint. Discussion started: 27 March 2026

2 Overall Architecture of the XCP

The operational schematic of the XCP is illustrated in Figure 1. The system comprises a buoy and a probe, with the probe housed at the lower end of the buoy. Upon deployment into the ocean, the probe is released and collects ocean current data as it descends. This data is transmitted via a dual-coat enamelled wire to the buoy or deck unit. The buoy then utilizes a wireless communication module to transmit the data in real-time to the receiving unit located on the ship or aircraft.

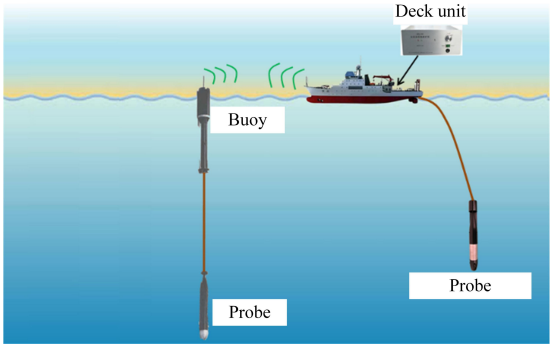

Figure 1: Operational schematic of the XCP.

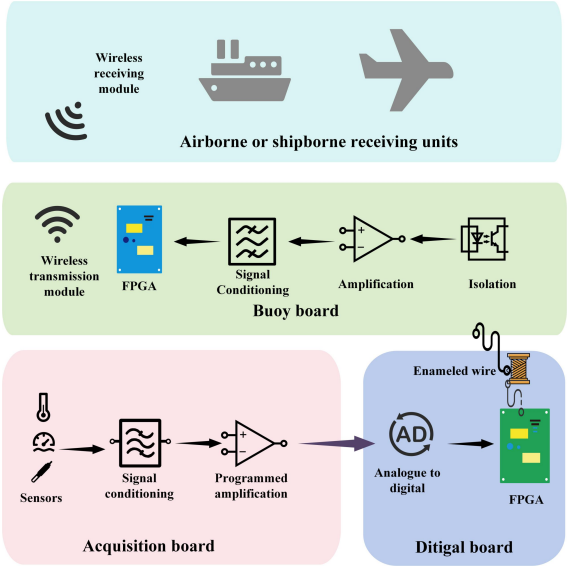

Figure 2: Overall block diagram of the XCP.

Figure 2 depicts the overall block diagram of the XCP. The system includes a sensor module, a probe section, a buoy section, and a receiving unit. The sensor module is tasked with measuring parameters such as temperature, salinity, depth, and ocean currents. The probe section consists of an analog board and a digital board. The analog board processes and amplifies the electrical signals collected by the sensors, which are then transmitted to the digital board for analog-to-digital conversion. The processed digital signals are subsequently transmitted to the buoy via a dual-coat enamelled wire through an FPGA. Upon receiving the high-noise LVDS signals from the enamelled wire, the buoy performs signal conditioning to

https://doi.org/10.5194/egusphere-2025-5066
Preprint. Discussion started: 27 March 2026

recover the data and sends it to the main control chip within the buoy unit for further processing. Finally, the data is wirelessly transmitted to the receiving device on the ship or aircraft, enabling efficient collection and transmission of marine environmental parameters.

3 Hardware Design for Data Transmission of the XCP

3.1. Dynamic Data Transmission Based on LVDS

Due to the unique characteristics of the XCP, data transmission in seawater requires the use of a dual-coat enamelled wire with a radius of 0.05mm and a length of 2500m (as shown in Figure 3). Practical tests have demonstrated that most transmission technologies are unable to achieve long-distance signal transmission over enamelled wire. Therefore, after extensive experimental testing, an LVDS-based data transmission method was selected.

The probe collects various signals, including electrode signals, compass coil signals, and temperature data, which are processed by the SOPC. The processed data is then transmitted using the UART protocol, which features a start bit of 1 bit, data bits of 8 bits, and a stop bit of 1 bit. Additionally, RS encoding is employed for data encoding, with the baud rate set to 9600. The transmitting end utilizes the LVDS (Bi et al., 2021) transmitter integrated within the SOPC to convert the signals into LVDS (Van et al., 2016) format for transmission over the enamelled wire.

Figure 3: Dual-coat enamelled wire: coiled (left) and uncoiled (right).

3.2. Hardware Circuit Design for the Receiving End

The principle block diagram of dynamic data transmission is illustrated in Figure 4. During the descent of the probe, the enamelled wire used for dynamic data transmission is in a state of rapid automatic unwinding. Initially, the enamelled wire is wound together, exhibiting inductive characteristics. As the descent progresses, however, the capacitance of the enamelled wire gradually increases. Additionally, the dielectric constant of seawater is relatively high, approximately 80 (David et al., 2022), which results in a significant amount of noise superimposed on the low-voltage differential signals transmitted through the enamelled wire. Upon reaching the buoy unit, the data transmitted through the enamelled wire is first isolated and amplified via a transformer to ensure no electrical connection between the enamelled wire and the buoy unit, thereby minimizing additional noise. The signals then pass through a high-pass filter circuit, a low-pass filter circuit, a hysteresis comparator, and an arithmetic circuit (the schematic of the buoy receiving end signal conditioning circuit is shown in Figure 5). These steps facilitate data recovery, which is then fed into the main control chip of the buoy unit for further processing.

https://doi.org/10.5194/egusphere-2025-5066
Preprint. Discussion started: 27 March 2026

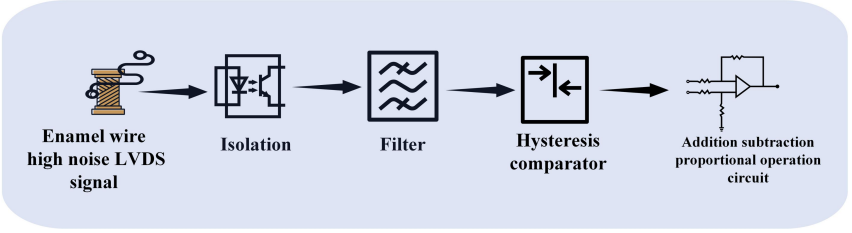

Figure 4: Principle block diagram of the dynamic data transmission conditioning circuit.

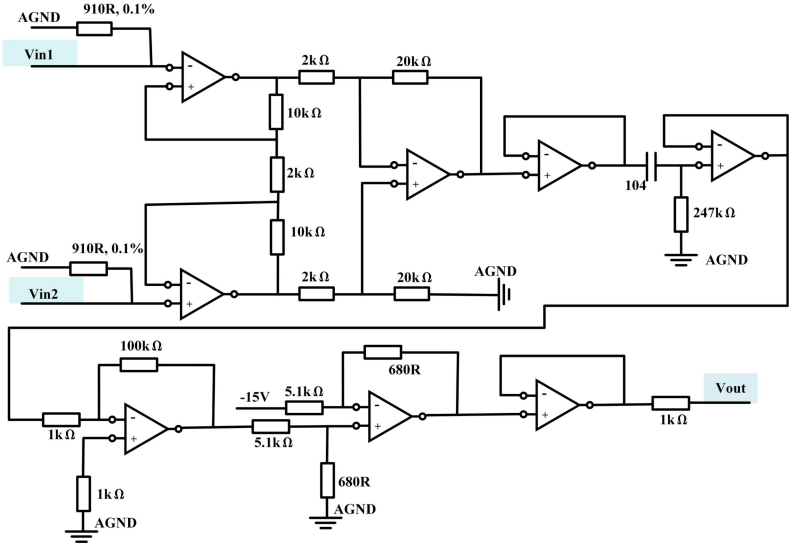

Figure 5: Schematic of the buoy receiving end signal conditioning circuit.

The original AC coupling circuit of the buoy data transmission receiving front end (as illustrated in Figure 6) had an issue where it did not provide a DC path for the bias current. This lack of a DC path could result in instability of the bias current and signal distortion. To mitigate these issues, two resistors can be added to ground on the output side of the transformer (as shown in Figure 7), or the centre tap of the transformer's output side can be grounded. These modifications ensure a stable DC path for the bias current, thereby reducing signal distortion and enhancing the accuracy and stability of data transmission. Testing the improved buoy circuit for enamelled wire data transmission has demonstrated that it can effectively achieve the intended objectives.

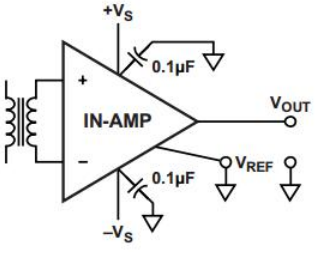

Figure 6: Unmodified transformer-coupled instrumentation amplifier circuit.

https://doi.org/10.5194/egusphere-2025-5066
Preprint. Discussion started: 27 March 2026

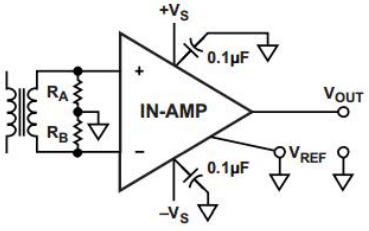

Figure 7: Improved transformer input coupling for instrumentation amplifier.

4 Software Design for Data Transmission of the XCP

4.1. Overall Software Design

The digital main control chip employs the Cyclone series FPGA from ALTERA. VHDL programming is used to generate trigger signals and implement various counting modules. Utilizing System-on-a-Programmable-Chip (SOPC) technology, the NIOS II soft core is embedded within the FPGA to control the probe's data acquisition process and data transmission. The control code for the NIOS II embedded processor is written in C, enabling the calculation and transmission of parameters such as electric field, coil, pressure, and temperature. SOPC integrates the entire embedded system onto a single chip, offering greater flexibility compared to System-on-Chip (SoC) designs, as users can expand or reduce functionalities based on their specific needs. SOPC design involves both C language software centered around the processor and hardware circuit design, achieving a seamless hardware-software co-design.

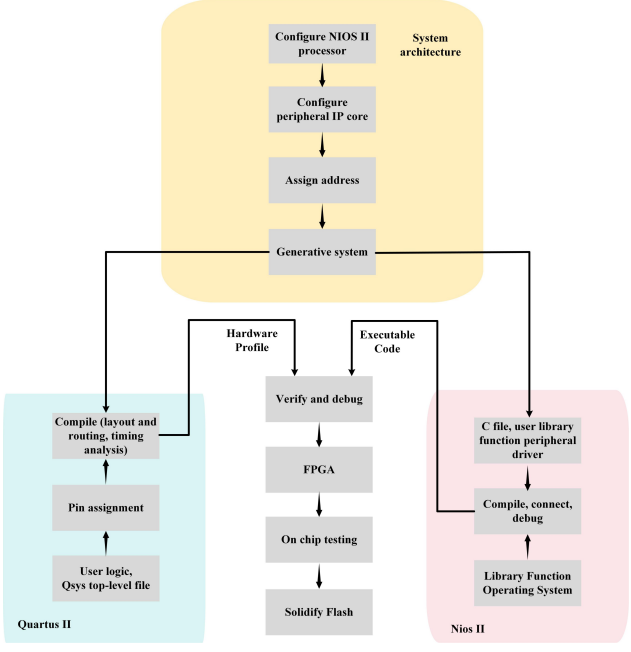

Figure 8. Overall flowchart of soft-core development.

https://doi.org/10.5194/egusphere-2025-5066
Preprint. Discussion started: 27 March 2026

Hardware design based on Quartus II and SOPC Builder typically includes configuring the NIOS processor, designing user logic, adding and configuring peripheral IP cores, and performing timing analysis. Additionally, application development, peripheral driver writing, and operating system execution are carried out using NIOS II Eclipse. The overall process flowchart is shown in Figure 8.

4.2. Overall Software Design

RS (Reed-Solomon) encoding and decoding is a widely used error-correcting coding technique that achieves error correction by adding redundant check codes. RS encoding is a type of cyclic redundancy check code that operates over a finite field GF(2^m). The redundant check codes in RS encoding are generated using a generator polynomial, while RS decoding employs syndrome and XOR operations to correct errors. The algorithms for RS encoding and decoding are characterized by their simplicity, reliability, and efficiency, making them extensively used in data transmission and storage applications. This technique ensures data integrity and robustness in various communication systems.

4.2.1. Principle of RS Encoding

In RS (Reed-Solomon) encoding, data is encoded according to specific rules, and redundant check codes are added. Upon receiving the encoded data, the recipient can perform decoding operations to detect and correct errors in the data. The generator polynomial for RS encoding can be calculated using the following formula:

$$G(x) = (x-\alpha)(x-\alpha^2)(x-\alpha^3).....\left(x-\alpha^{n-k}\right) \quad (1)$$

Generally, α is a primitive element in the finite field GF(2^m). The code length n is (2^m-1) symbols, the information segment is k symbols, and the parity segment $2t=n-k$ symbols, where t is the maximum number of errors that can be corrected by the RS code. The fundamental idea of RS coding is that, based on the generated polynomial $G(x)$, each codeword polynomial computed from an information segment is a multiple of $G(x)$. Thus, when the codeword polynomial is divided by $G(x)$, the remainder should be zero. If the remainder is not zero, it indicates the presence of errors, which can be corrected up to $t=(n-k)/2$ errors (Gao et al., 2021). Assuming the codeword polynomial is $C(x)$, the remainder is $R(x)$, the quotient is $H(x)$, and the information segment polynomial is $D(x)$, we have the following relationship:

$$x^{n-k} \cdot \frac{\mathrm{D}(x)}{\mathrm{G}(x)} = H(x) \cdot G(x) + R(x) \quad (2)$$

We can set the remainder $R(x)$ as the check symbols, thus:

$$C(x) = x^{n-k} \cdot \mathrm{D}(x) + \mathrm{R}(x) \quad (3)$$

Therefore, the codeword polynomial divided by the generator polynomial can be expressed as:

$$\frac{C(x)}{G(x)} = x^{n-k} \cdot \frac{D(x)}{G(x)} + \frac{R(x)}{G(x)} = H(x) \cdot G(x) + R(x) + \frac{R(x)}{G(x)} = H(x) \cdot G(x) \quad (4)$$

Therefore, the codeword polynomial $C(x)$ must be divisible by the generator polynomial $G(x)$, as the remainder $R(x)$ is zero. If the remainder is detected to be non-zero, it indicates that the two polynomials are not divisible, signifying the

https://doi.org/10.5194/egusphere-2025-5066
Preprint. Discussion started: 27 March 2026

presence of erroneous codewords that need correction. Due to the characteristics of RS codes, they are particularly well-suited for channels with burst errors.

4.2.2. Principle of RS Encoding

Upon receiving the encoded data, the receiver must perform decoding operations to detect and correct any errors in the data. RS decoding is accomplished using syndrome and XOR operations. The decoding process can be divided into the following steps (Li et al., 2020):

1. Perform XOR operations on the received encoded data to obtain the syndrome polynomial $e(x)$.
2. Use the syndrome to calculate the error locator polynomial $\sigma(x)$.
3. Calculate the error value polynomial $\omega(x)$ using the error locator polynomial $\sigma(x)$.
4. Perform XOR operations between the error value polynomial $\omega(x)$ and the received encoded data to obtain the corrected data.
5. A critical step in decoding is determining the error locator polynomial. Common algorithms for solving this set of equations include the Euclid algorithm and the Berlekamp-Massey algorithm.

These steps ensure that errors in the received data can be accurately located and corrected, thereby restoring the original information. The robust error correction capabilities of RS codes make them particularly suitable for channels prone to burst errors.

4.2.3. Design and Implementation of RS Encoding and Decoding IP Core

The RS encoding and decoding IP core is a hardware-based module that can be directly integrated into an FPGA chip, ensuring efficient and reliable data transmission and storage (Samanta et al., 2017; Gao et al., 2021). This paper presents the design of an RS encoding and decoding IP core based on FPGA, implemented using Verilog language. The design of the RS encoding and decoding IP core primarily consists of two components: the encoder and the decoder. The encoder encodes the input data and generates redundant check codes, while the decoder decodes the received data to recover the original information.

Upon completing the IP core setup, we utilized Modelsim software to simulate its functionality and verify its performance through waveform analysis. The simulation was run for 10μs, and the results were observed. The RS encoding Modelsim simulation waveform is shown in Figure 9. From the waveform, we can observe the following signals:

- clk: Clock signal
- reset: Reset signal
- sink_ena: Input feedback signal, indicating the encoding state when high
- sink_eop: End of input signal transmission
- sink_sop: Start of input signal transmission

https://doi.org/10.5194/egusphere-2025-5066
Preprint. Discussion started: 27 March 2026

- sink_val: Enable signal
- rsin: Input data value before encoding
- source_ena: Output feedback signal
- source_eop: End of output signal transmission
- source_sop: Start of output signal transmission
- source_val: Enable signal
- rsout: Output data after encoding

The waveform analysis confirms that the designed encoding circuit meets the expected requirements.

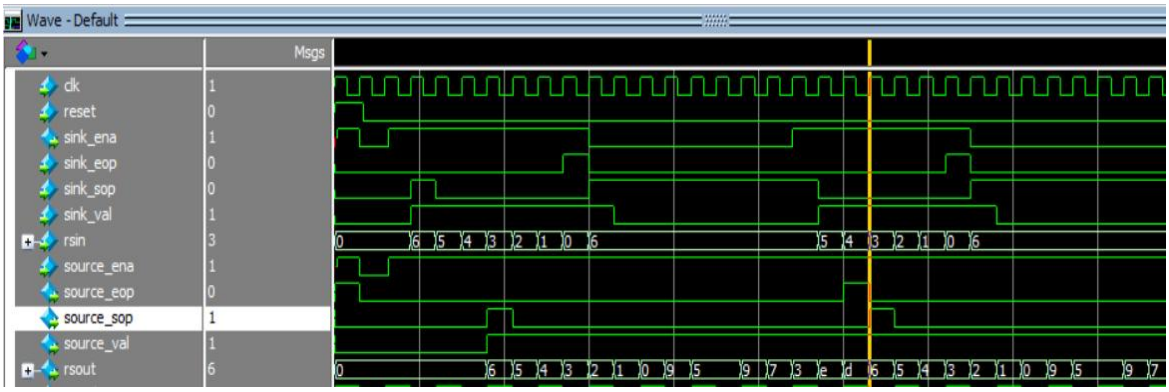

Figure 9: ModelSim simulation waveform of RS encoding. (©ModelSim)

The setup of the RS decoder IP core (Li et al., 2003) is similar to that of the encoder. During simulation, the decoder file needs to be added in Modelsim for verification, and the simulation should be run for 20 s to observe the waveform. In the decoding waveform, several new signal waveforms are introduced:

- bypass: Indicates the signal channel.
- num_err_sym: Represents the number of erroneous codewords in a data sequence. In this design, the maximum error correction capability is 4, so if the number of erroneous codewords exceeds 4, this waveform will show a maximum value of 4, and the decfail signal will be asserted, indicating a decoding failure.
- decfail: Indicates a decoding failure when asserted.
- rserr: Provides the auxiliary value for correcting erroneous codewords. By performing an XOR operation between this value and the input erroneous code, the erroneous codewords can be corrected, thereby outputting the correct codewords and completing the error correction function.

Figure 10 shows the waveform for a decoding failure. Based on Figure 10, it can be observed that data transmission begins when the sink_sop signal is asserted high and stops when the sink_eop signal is asserted high. At the output port, data transmission starts when the source_sop signal is asserted high and completes when the source_eop signal is asserted high. In the first set of data, the actual transmitted values are 02, 04, 06, 08, 10, 12, 14, 00, 12, 03, 05, 13, 03, 04, 00. However, the input data for decoding contains errors: 02, 04, 06, 08, 10, 12, 00, 03, 14, 03, 05, 13, 03, 00, 02. There are 5 erroneous

https://doi.org/10.5194/egusphere-2025-5066
Preprint. Discussion started: 27 March 2026

codewords in this sequence, which exceeds the error correction capability of the code. Consequently, the rsout port outputs erroneous data, the num_err_sym signal shows the maximum error correction value of 4, and the decfail signal is asserted high, indicating a decoding failure. Figure 11 shows the waveform for a successful decoding.

Based on Figure11, it can be observed that data transmission begins when the sink_sop signal is asserted high and stops when the sink_eop signal is asserted high. At the output port, data transmission starts when the source_sop signal is asserted high and completes when the source_eop signal is asserted high. From the figure, it can be seen that num_err_sym indicates 2, and the decfail signal remains low, signifying that the output data contains two erroneous codewords. According to the values provided by the rserr waveform, the erroneous codewords are located at the 7th and 11th positions. By performing XOR operations between the rserr values 14 (binary: 1110) and 3 (binary: 0011) with the input erroneous codeword values 8 (binary: 1000) and 11 (binary: 1011), the correct codewords 6 (binary: 0110) and 8 (binary: 1000) are obtained. Thus, the correct transmitted data values are 00, 01, 02, 03, 04, 05, 06, 07, 00, 06, 08, 11, 15, 08, 02.

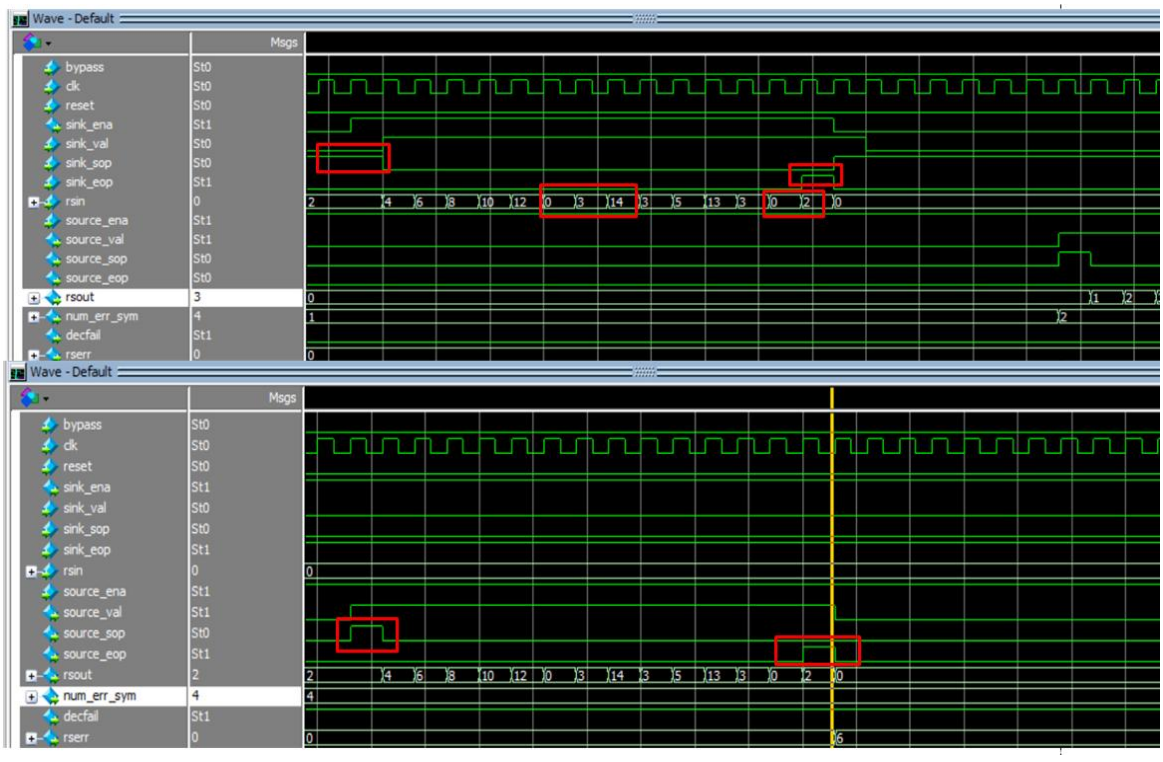

Figure 10: RS decoding failure waveform. (©ModelSim)

https://doi.org/10.5194/egusphere-2025-5066
Preprint. Discussion started: 27 March 2026

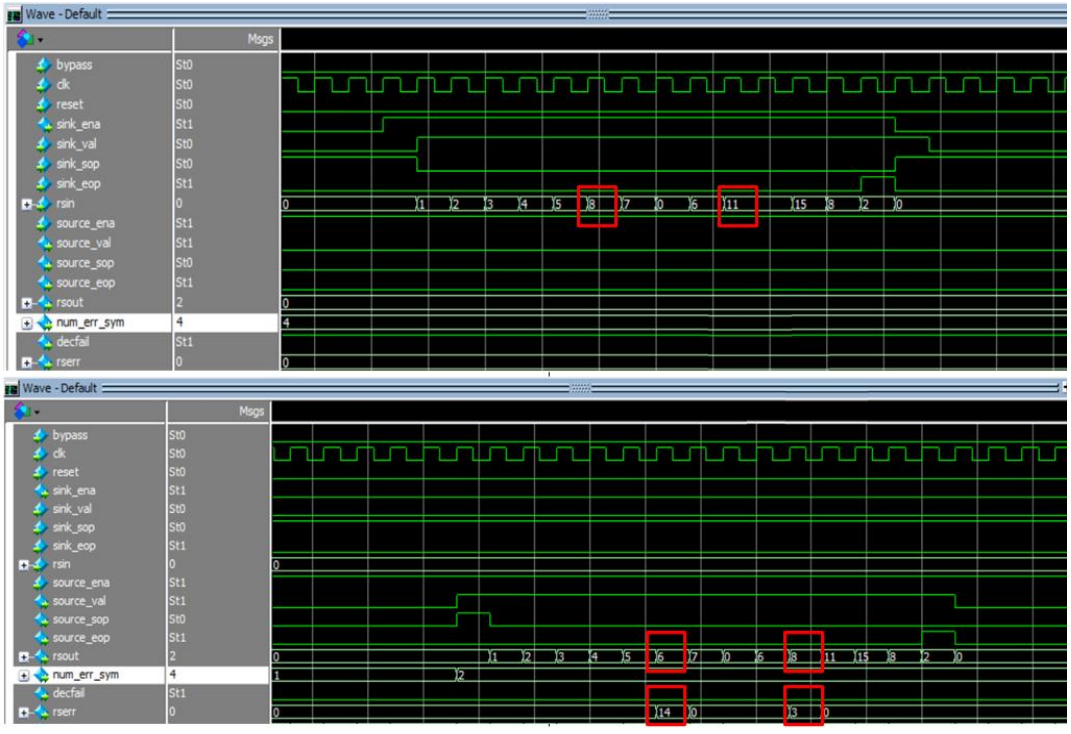

Figure 11: RS decoding successful waveform. (©ModelSim)

5. Instrument Testing

Firstly, we conducted enamelled wire data transmission experiments to verify the feasibility of this data transmission method in marine environments. The experimental results indicate that when the length of the enamelled wire is less than 2500 meters, effective data transmission can be achieved using both the transformer centre tap grounding method and connecting 10 kΩ resistors to ground at the input end.

Secondly, comprehensive testing of the XCP system was carried out at the Beihai Monitoring Centre in Qingdao, Shandong, to further validate the application of this data transmission method in expendable marine profilers. The test results demonstrate that data transmission over a 2500-meter enamelled wire at a baud rate of 9600 bps is feasible. Additionally, MATLAB simulations of RS (15, 7) encoding and decoding were performed to assess the bit error rate, showing that a bit error rate of 10^{-4} can be achieved at a signal-to-noise ratio of 12 dB.

Lastly, tests were conducted in the lab and electromagnetic shielding room. These tests simulated the marine environment and weak signal conditions to verify the ability of the XCP to measure extremely weak signals in a noise-free environment. The experimental results showed a good linear relationship between the electrode voltage and the copper plate voltage, confirming the accuracy of the data collected by the XCP and further validating the feasibility of this data transmission method.

https://doi.org/10.5194/egusphere-2025-5066
Preprint. Discussion started: 27 March 2026

Through these experiments, we confirmed the effectiveness of data transmission and measurement accuracy of the XCP probe in practical applications.

5.1. Enamelled Wire Data Transmission Experiment

The original AC coupling circuit at the receiving front end of the buoy data transmission system had an issue where it did not provide a DC path for the bias current. Using the improved buoy circuit, we conducted data transmission experiments with enamelled wires of different lengths and conditions. The test setup is shown in Figure 12, and the results are presented in Table 1. It can be observed that, for enamelled wire lengths less than 2500 meters, both the method of grounding the centre tap of the transformer's output side and the method of connecting 10 kΩ resistors to ground at the output side enable normal data transmission.

For the case where data transmission failed on a 2700-meter coiled enamelled wire, we used a signal generator to apply a pair of differential signals with a frequency of 10 kHz and a peak-to-peak value of 3 V to the enamelled wire. Measurements on the other side of the enamelled wire showed that the signals on the two wires were nearly identical. This indicates that the failure of data transmission over the 2700-meter enamelled wire was due to the differential signals losing their differential characteristics after traveling through the coiled wire, making it impossible for the buoy to decode the signals.

These experiments demonstrate the effectiveness of the improved buoy circuit and highlight the limitations of data transmission over excessively long enamelled wires.

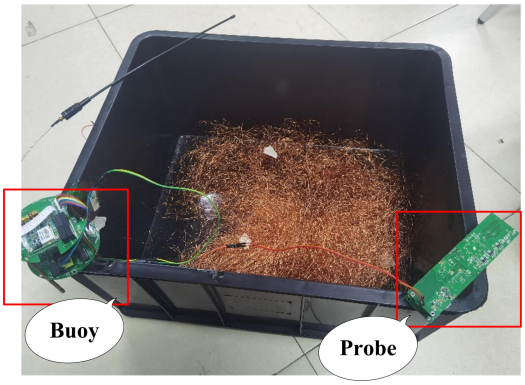

Figure 12: Enamelled wire data transmission experiment setup.

Table 1. Enamelled wire data transmission experiment results.

Buoy Input Condition	Enamelled Wire Condition	Data Transmission Result
Transformer centre tap grounded	100 m uncoiled	Successful
10 kΩ resistors to ground at input	100 m uncoiled	Successful
10 kΩ resistors to ground at input	1000 m uncoiled	Successful
10 kΩ resistors to ground at input	1000 m uncoiled and immersed in saltwater	Successful
10 kΩ resistors to ground at input	2500 m uncoiled and immersed in saltwater	Successful

https://doi.org/10.5194/egusphere-2025-5066
Preprint. Discussion started: 27 March 2026

10 kΩ resistors to ground at input	500 m coiled and immersed in saltwater	Successful
10 kΩ resistors to ground at input	2500 m coiled and immersed in saltwater	Successful
10 kΩ resistors to ground at input	500 m coiled + 100 m uncoiled and immersed in saltwater	Successful
Transformer centre tap grounded	500 m coiled + 100 m uncoiled and immersed in saltwater	Successful
10 kΩ resistors to ground at input	500 m coiled + 1000 m uncoiled and immersed in saltwater	Successful
Transformer centre tap grounded	2700 m coiled	Unsuccessful
10 kΩ resistors to ground at input	2700 m coiled	Unsuccessful

5.2. Enamelled Wire Data Transmission Experiment

A testing environment was set up at the Beihai Monitoring Center in Qingdao, Shandong, China, using real seawater to conduct probe air-tightness, rotation tests, and LVDS data transmission tests, as shown in Figure 13. The data transmission lines of the probe were connected to the buoy using conductive slip rings to perform the data transmission test. The results demonstrated that the XCP system could effectively transmit data through the enamelled wire in a real marine environment. The successful implementation of these tests further validates the reliability and robustness of the data transmission method used in the expendable marine profiler.

Figure 13: Probe rotation test.

A comprehensive XCP system structure was set up to conduct data transmission experiments and verify whether the transmission baud rate could reach 9600 bps. The probe was connected to the enamelled wire, which was then connected to the buoy board. Subsequently, the data was transmitted wirelessly to the host computer for display. As shown in Figure 14, the corresponding serial port of the wireless module was selected, and the reception baud rate was set to 9600 bps. The serial port was then opened to check whether the data was being transmitted correctly. The actual results demonstrate that normal data transmission can be achieved at a baud rate of 9600 bps over a 2500-meter enamelled wire.

https://doi.org/10.5194/egusphere-2025-5066
Preprint. Discussion started: 27 March 2026

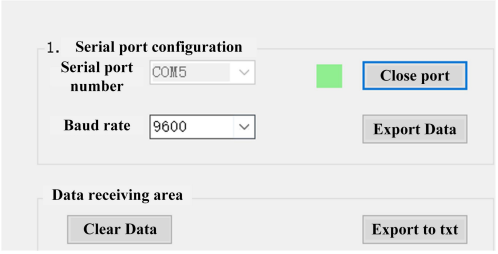

Figure 14: Serial port and baud rate settings.

Using MATLAB software, we wrote code to simulate the bit error rate (BER) of RS (15, 7) encoding and decoding, which allowed us to plot the BER curve (Figure 15). In this plot, the vertical axis represents the bit error rate (BER), and the horizontal axis represents the signal-to-noise ratio (SNR) in decibels (dB). From the graph, we can see that when the SNR is 12 dB, the BER of the encoding reaches 10^{-4}.

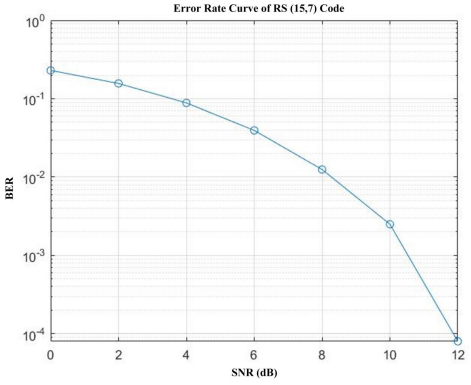

Figure 15: BER Curve for RS (15, 7) Encoding and Decoding.

5.3. Simulated Testing of XCP

According to the signal characteristics of marine currents, during the actual dynamic measurement of marine current velocity, the probe of the XCP is required to rotate during its descent, with the rotational speed converging to a stable frequency, which ensures the marine current signal is converted into an approximately stable single-frequency signal (Zhou et al., 2023). Meanwhile, based on the measurement principle of weak marine current signals, the laboratory setup for simulating the marine current environment is divided into two parts: one is an electric field environment composed of a non-metallic water tank filled with seawater, two conductive copper plates, a DC stabilized power supply, a lock-in amplifier, and a precision attenuator, where the simulated seawater is a saline solution with a concentration of 3.5% and the conductive copper plates are placed in relative parallelism; the other is a rotation device consisting of a small DC motor, a motor speed controller, and a rotational bracket for the expendable probe, which can simulate the acquisition process of the expendable probe's rotational descent. A schematic diagram of the indoor simulated marine electric field environment is shown in Figure 16.

https://doi.org/10.5194/egusphere-2025-5066
Preprint. Discussion started: 27 March 2026

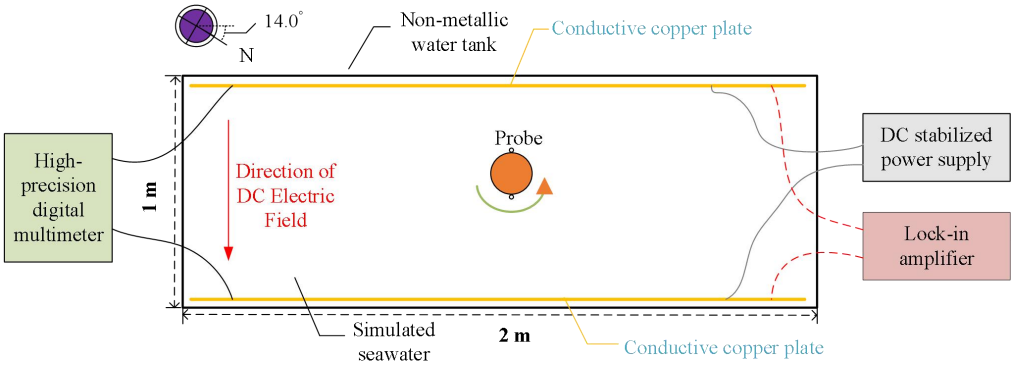

Figure 16: Schematic diagram of marine current simulation environment construction.

Therefore, based on the measurement principle of XCP, two simulation test methods can be adopted in the indoor simulated environment to test and analyze: one is the marine current signal simulation test under a DC electric field (active source), and the other is the ocean current signal simulation test under an AC electric field (passive source).

When a DC stabilized power supply is used to power the copper plates, the two powered copper plates form a stable DC electric field environment through seawater. This stable DC electric field environment is constructed to replace the electric field generated by the cutting of the geomagnetic field by ocean current movement; meanwhile, a rotation device is used to modulate the ocean current signal. In contrast, when a lock-in amplifier and a precision attenuator are employed to provide a stable AC signal to the copper plates, a stable AC electric field environment is formed between the two plates. This AC electric field environment is constructed to simulate the rotational acquisition of induced electric field signals by XCP in practical scenarios. Consequently, no rotation device is required for assistance in the AC electric field environment.

Through the above two indoor simulation test methods for the current acquisition module, two objectives can be achieved: on the one hand, they can verify the data transmission capability of XCP and its ability to capture weak electric field signals; on the other hand, they can better simulate the process of the probe acquiring marine current signals in the actual sea trial environment.

5.3.1. Active Source Simulation Testing

The construction of the indoor marine current simulation environment mainly consists of four components (Figure 17(a)): conductive copper plates, a plastic water tank, simulated seawater, and a probe rotation device. Among these, two oppositely placed copper plates are used to simulate the electric field generated by marine currents cutting the geomagnetic field, while the probe rotation device can drive the expendable probe to rotate at a stable frequency.

In Figure17 (b), a DC power supply, a lock-in amplifier, a precision attenuator, a digital multimeter, and an oscilloscope together form the signal sources and monitoring equipment of the indoor marine current simulation environment. Specifically, the DC power supply provides a DC signal source for DC electric field experiments; the lock-in amplifier and

https://doi.org/10.5194/egusphere-2025-5066
Preprint. Discussion started: 27 March 2026

precision attenuator provide AC signal sources for AC electric field experiments; and the digital multimeter and oscilloscope enable real-time signal monitoring.

(a) (b)

Figure 17: The laboratory simulates the construction of the test environment:(a) Simulate marine current electric fields and probe fixtures; (b) Analog signal sources for marine currents and monitoring equipment

During the acquisition process, different acquisition experiments were set up by adjusting the output of the DC power supply, and multiple sets of experimental acquisition data were thereby obtained. Since the DC power supply is used to simulate the measured ocean current electric field signal and its output voltage is relatively low, a high-precision digital multimeter was employed to monitor the voltage of the copper plates in real time under different DC power supply outputs. Meanwhile, the data transmitted back by the XCP was stored promptly. After the completion of the DC electric field acquisition test, the experimental data were organized, as shown in Figure 18.

The experimental results indicate that as the copper plate voltage increased from 8 mVrms to 20 mVrms, the measured value of the induced electric field increased continuously and exhibited an approximately linear relationship with the copper plate voltage, before gradually tending toward saturation. In contrast, when the output voltage of the DC power supply was less than 8 mVrms, the electrode voltage acquired by the XCP showed instability. This phenomenon suggests that there is noise interference in the current indoor environment, which poses considerable challenges to the extraction of weak ocean current signals at this magnitude. However, such environmental noise does not exist in the actual marine environment.

Furthermore, this experiment verifies that based on the designed digital transmission technology, the system can still achieve stable and reliable data transmission under the conditions of an enameled wire with a radius of 0.05 mm and a length of 2500 meters, at a transmission baud rate of 9600 bps. Meanwhile, the normal operation of the signal acquisition function is guaranteed, which fully demonstrates that the entire data transmission and acquisition system possesses technical feasibility and application potential.

https://doi.org/10.5194/egusphere-2025-5066
Preprint. Discussion started: 27 March 2026

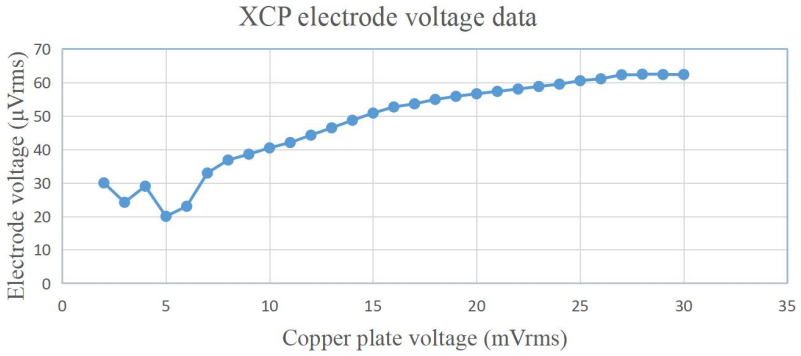

Figure 18: DC electric field test results.

5.3.2. Passive Source Simulation Testing

We conducted experiments to measure weak signals using the XCP probe inside an electromagnetic shielding room. This setup eliminates external electromagnetic interference and verifies the XCP probe's capability to measure weak signals and data transmission. The experiments were carried out at the electromagnetic shielding room of the Huailai Remote Sensing Comprehensive Test Station, Chinese Academy of Sciences, in Beijing, China. The dimensions of the shielding room are 2 meters in length, 2 meters in width, and 2 meters in height. The room has three metal conduits on its sides, through which cables can be routed.

Due to the extremely weak signals collected by the XCP probe, we used a signal generator to output millivolt-level signals and incorporated a resistive voltage divider attenuation circuit at the front end of the acquisition board to attenuate the signals to the microvolt level. We also considered the thermal noise of the resistors in the attenuation circuit. Under a fixed bandwidth, the larger the resistance value, the greater the thermal noise. Therefore, we used resistors with values within 1 kΩ for attenuation. The experimental setup is shown in Figure 19. The small water tank is 50 cm long, 30 cm wide, and 40 cm high. It was filled with 20 cm deep tap water, and 1300g of sea salt was added to simulate a seawater environment. Two 25 cm wide copper plates were placed in the tank, leaning against the inner walls of the short sides of the tank. The enamelled wire was routed through the metal conduits on the side of the electromagnetic shielding room, and data was parsed and analyzed outside the shielding room.

Figure 19: Experimental setup.

https://doi.org/10.5194/egusphere-2025-5066
Preprint. Discussion started: 27 March 2026

A lock-in amplifier generates an alternating electric field in the water tank through copper plates, and the XCP probe collects the electric field signals in the water via electrodes, recording the measurement data of the XCP probe at different copper plate voltages.

The relationship between the electrode voltage measured by the XCP probe and the copper plate voltage is shown in Figure 20. The measured electrode voltage decreases as the copper plate voltage decreases. The lock-in amplifier shows a good linear relationship between the electrode signal and the copper plate voltage, with a few anomalies at low voltages. These anomalies are likely due to the extremely weak signals, where minor noise interference from the metal conduits on the side of the shielding room might have coupled into the signal lines, affecting the quality of the copper plate voltage signals and, consequently, the XCP's measurement of the electric field in the water. Through this experiment, we verified that the XCP probe can accurately measure weak electric field signals in an interference-free environment. However, at extremely low voltages, external noise interference needs to be considered. These results demonstrate the high reliability and accuracy of the XCP probe in measuring very weak signals and also validate the feasibility and accuracy of the data transmission method.

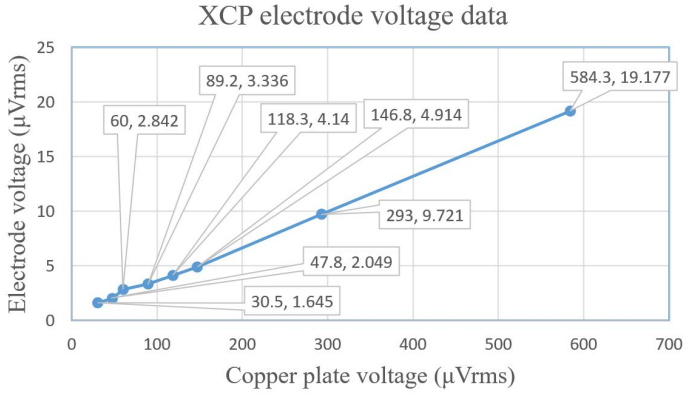

Figure 20: Relationship between Electrode Voltage Measured by XCP and Copper Plate Voltage.

6. Conclusions

This paper analyzed the data acquisition process of the XCP, optimized and improved the analog board circuit to enable more precise data collection by the probe, thus reducing interference. RS encoding technology was added to the digital board of the probe to lower the transmission error rate, and the hardware description language code for the improved probe control unit was developed. By analyzing the dynamic data transmission method of XCP, the transmission method was optimized and improved. This involved providing a DC path for the bias current of the AC coupling circuit at the receiving end of the differential signal on the output end, thereby increasing the data transmission rate of the expendable current profiler. The

https://doi.org/10.5194/egusphere-2025-5066
Preprint. Discussion started: 27 March 2026

ultimate goal was to achieve faster and more accurate ocean current information detection. Using devices such as a water tank and copper plates, a simulated environment for actual marine testing of the XCP was constructed. Specifically:

1. **Hardware Circuit Optimization**: The analog circuit design for LVDS data transmission was optimized, processing the LVDS signals with superimposed noise and transmitting them to the deck unit via a wireless module to reduce interference. Additionally, the hardware description language code for the improved probe control unit was developed, further enhancing system performance.
2. **Dynamic Data Transmission Optimization**: By analyzing the dynamic data transmission method of the expendable current profiler, optimizations and improvements were made. Specifically, a DC path was provided for the bias current of the AC coupling circuit at the receiving end of the differential signal on the output end, reducing garbled data and improving data transmission quality, enabling faster and more accurate ocean current information detection.
3. **Experimental Verification**: Using devices such as a water tank, a simulated marine testing environment for the XCP was constructed. The data transmission rate on a 2500-meter enamelled wire was increased to 9600 bps, making the data points collected by the instrument denser and ensuring data reliability.
4. **Software Program Design**: Control of the probe acquisition process and data transmission was implemented using VHDL hardware description language. Processor control code was written in C language for the NIOS II soft core, achieving the transmission of parameters such as electric field, coil, and temperature. Additionally, RS encoding and decoding functionality was introduced into data transmission, reducing the error rate to 10^{-4}, significantly increasing data transmission speed while ensuring data accuracy.
5. **System Performance Testing**: Board-level debugging of the XCP probe, buoy analog board, and digital board was completed, along with related functional tests in an indoor environment. After assembling the entire XCP system and conducting integrated testing, testing environments were set up in both the shielding room and the Beihai Monitoring Center to test the overall performance of the probe. The results indicated that all functions of the design operated normally and stably, achieving the expected outcomes.

In summary, this paper designed and implemented an XCP based on improved dynamic data transmission technology, significantly enhancing data transmission speed and accuracy. This provides reliable technical support for the efficient collection and transmission of marine environmental parameters. Future research will continue to explore deeper ocean areas, multi-parameter synchronous measurement, data processing and analysis, energy management optimization, and modular design to further improve the performance and application value of the equipment.

Code and data availability

The original contributions presented in the study are included in the article, further inquiries can be directed to the corresponding author.

https://doi.org/10.5194/egusphere-2025-5066
Preprint. Discussion started: 27 March 2026

Author contributions

F.Z., L.L., Z.P., D.L.(Donghui Li), D.L.(Dong Liu), Q.Z., K.Z. and X.J. designed the whole system, experiments and carried them out. K.Z. prepared the manuscript with contributions from all co-authors.

Competing interests

The authors declare that they have no conflicts of interest.

Acknowledgment

We would like to express our gratitude to China University of Geosciences (Beijing), Shandong University of Science and Technology, Beihai Environmental Monitoring Center of the Ministry of Natural Resources of the People's Republic of China, and Huailai Remote Sensing Comprehensive Test Station of the Chinese Academy of Sciences for providing an excellent testing environment.

Financial support

This research received support from the National Key R & D Program of China (Grant No. 2022YFF0607505) and the National Natural Science Foundation of China (Grant Nos. 42576081, U22A2012).

References

Alvarinho J. LuisCA1,2;Vinit R. Lotlikar.Hydrographic characteristics along two XCTD sections between Africa and Antarctica during austral summer 2018[J].Polar Science,2021,Vol.30: 100705

Bi, Yan-Feng;Li, Jie;Hu, Chen-Jun;Gao, Ning;Gao, Shi-Yao.Design and Implementation of Speed Adaptive Data Readback System Based on LVDS[J].Zhongbei Daxue Xuebao (Ziran Kexue Ban)/Journal of North University of China (Natural Science Edition),2021,Vol.42(1): 75-81

David M. Le Vine;Yiwen Zhou;Roger H. Lang.Model for Dielectric Constant of Seawater based on L-band Measurements with Conductivity by Definition[J].IEEE Geoscience and Remote Sensing Letters,2022,Vol.19: 1

Fan Hanbai;Liu Bingyue;Wu Fei;Li Ruiqi.Design of communication system for ocean expendable sound velocity meter(XSV)[J].Dianzi Jishu Yingyong,2019,Vol.45(7): 112-116

https://doi.org/10.5194/egusphere-2025-5066
Preprint. Discussion started: 27 March 2026

Hannon, J.;Institute of Electric and Electronic Engineer.New developments in expendable oceanographic sensors and data acquisition systems[A].OCEANS 2000 MTS/IEEE Conference and Exhibition. Conference Proceedings (Cat. No.00CH37158)[C],2000

Gao, Zhen;Zhang, Lingling;Cheng, Yinghao;Guo, Kangkang;Ullah, Anees;Reviriego, Pedro.Design of FPGA-Implemented Reed-Solomon Erasure Code (RS-EC) Decoders With Fault Detection and Location on User Memory[J].IEEE Transactions on Very Large Scale Integration (VLSI) Systems,2021,Vol.29(6): 1-10

Hongfeng Zhang;Baoxiang Huang;Ge Chen;Linyao Ge;Milena Radenkovic.An Efficient Oceanic Eddy Identification Method With XBT Data Using Transformer[J].IEEE Journal of Selected Topics in Applied Earth Observations and Remote Sensing,2022,Vol.15: 1-13

Justine Parks;Francis Bringas;Rebecca Cowley;Craig Hanstein;Lisa Krummel;Janet Sprintall;Lijing Cheng;Mauro Cirano;Samantha Cruz;Marlos Goes;Marlos Goes;Shoichi Kizu;Franco Reseghetti.XBT operational best practices for quality assurance[J].Frontiers in Marine Science,2022,Vol.9

Li, Hongzhi;Zhang, Sai;Qin, Xiaocong;Zhang, Xiaoyang;Zheng, Yu.Enhanced Data Transmission Rate of XCTD Profiler Based on OFDM[J].Journal of Ocean University of China. JOUC,2019,: 1-7

Long, Yu;Zhu, Xiao-HuaCAa;Guo, Xinyu;Ji, Fei;Li, Zhiyuan.Variations of the Kuroshio in the Luzon Strait Revealed by EOF Analysis of Repeated XBT Data and Sea-Level Anomalies[J].Journal of Geophysical Research: Oceans,2021,Vol.126(7)

Li Jinming;Liu Mengxin;Cheng Naipeng.Optimization and FPGA implementation of RS coding algorithm[J].Dianzi Jishu Yingyong,2020,Vol.46(2): 76-79

Qisheng Zhang, Ming Deng, Qi Wang, Yongqiang Feng, Rui Yang. Dynamic Data Transmission Technique for Expendable Current Profiler[J]. Advanded Materials Research Vols.219-220(2011) : 436-440.

Li, X.-C.;Shen, B.-S..Design and implementation of RS encoding and decoding on FPGA(Article)[J].Tianjin Daxue Xuebao (Ziran Kexue yu Gongcheng Jishu Ban)/Journal of Tianjin University Science and Technology,2003,Vol.36(2): 220-224

Sanford,T.B.:Motionally induced electric and magnetic fields in the sea, J. Geophys. Res.-Oceans., 76, 3476–3492,https://doi.org/10.1029/JC076i015p03476, 1971.

Sanford, T. B., Drever, R. G., and Dunlap, J. H.: A velocity profiler based on the principles of geomagnetic induction, Deep-Sea Res., 25, 183–210, https://doi.org/10.1016/01466291(78)90006-1, 1978.

https://doi.org/10.5194/egusphere-2025-5066
Preprint. Discussion started: 27 March 2026

Sijia Li;Hao Zhang;Jiajun Lu;Pengfei Wu;Wei Huang.Expendable Conductivity–Temperature–Depth-Assisted Fast Underwater Sound Speed Estimation by Convolutional Neural Network with Reduced Fully Connected Layers[J].Journal of Marine Science and Engineering,2024,Vol.12(3): 400

Samanta, J.;Bhaumik, J.;Barman, S..FPGA based area efficient RS(23, 17) codec[J].Microsystem Technologies,2017,Vol.23(3): 639-650

S. Li;S. Li;Q. Zhang;Q. Zhang;X. Zhao;X. Zhao;S. Liu;S. Liu;Z. Yuan;Z. Yuan.Dynamic data transmission technology for expendable current profiler based on low-voltage differential signaling[J].Geoscientific Instrumentation, Methods and Data Systems,2017,Vol.6(6): 263-267

Van Lingling;Wen Feng;Li Huijing.An interface optimization design based on LVDS high speed transmission[J].Electrical Measurement and Instrumentation,2016,Vol.53(20): 80-83

Zhou K, Chen G, Zhang Q, et al. Development of an expendable current profiler and simulation of passive sources[J]. Measurement Science and Technology, 2023, 34(8): 085903.

Zhou, K., Zhang, Q., Chen, G., Lin, Z., Liu, Y., and Li, P.: Development of an expendable current profiler based on modulation and demodulation[J]. Geosci. Instrum. Method. Data Syst., 12, 57–69, https://doi.org/10.5194/gi-12-57-2023, 2023.